



Contributions from intrinsic low-frequency climate variability to the accelerated decline in Arctic sea ice in recent decades

Lejiang Yu¹, Shiyuan Zhong²

5 ¹SOA Key Laboratory for Polar Science, Polar Research Institute of China, Shanghai, China

²Department of Geography, Environment and Spatial Sciences, Michigan State University, East Lansing, MI, USA

Correspondence to: Dr. Shiyuan Zhong (zhongs@msu.edu)



10 **Abstract.** In recent decades, the Arctic sea ice has been declining at a rapid pace as the Arctic is warmed
at a rate of twice the global average. The underlying physical mechanisms for the Arctic warming and
accelerated sea ice retreat are not fully understood. In this study, we apply a relatively novel statistical
method called Self-Organizing Maps (SOM) to examine the trend and variability of autumn Arctic sea
ice in the past four decades and their relationships to large-scale atmospheric circulation changes. Our
15 results show a large portion of the autumn Arctic sea ice decline between 1979 and 2016 may be
associated with anomalous autumn Arctic intrinsic atmospheric modes. The Arctic atmospheric
circulation anomalies associated with anomalous sea surface temperature patterns over the North Pacific
and North Atlantic influence Arctic sea ice primarily through anomalous temperature and water vapor
advection and associated radiative feedback.

20 **1 Introduction**

In recent decades, the Arctic sea ice has been decreasing at an unprecedented rate (Rothrock et al., 1999;
Parkinson, 2014). The accelerated retreat in Arctic sea ice exerts a significant impact not only on the
marine and terrestrial ecological systems of the Arctic (Post et al., 2013), but also on the environment of
the mid latitude (Mori et al., 2014; Kug et al., 2015).

25 The underlying mechanisms for the Arctic sea ice decline remain a subject of active research. Studies
have suggested that both anthropogenic forcing due to greenhouse gas and aerosol emissions (Min et al.,
2008; Notz and Marotzke, 2012; Gagné et al., 2015) and natural mechanisms at a wide range of scales
contribute to the observed Arctic sea ice decline. Local processes, including surface thermal inversion
(Bintanja et al., 2011), atmospheric lapse-rate (Pithan and Mauritsen, 2014), ice-albedo feedback
30 (Flanner et al., 2011) and water vapour and cloud radiative feedback (Sedlar et al., 2011), have been
found to affect Arctic sea ice. On the other end, global sea-surface temperature (SST) and pressure
oscillations, such as the Arctic Dipole (AD) (Wang et al., 2009), the Atlantic Multidecadal Oscillation
(AMO) (Park and Latif, 2009), the Arctic Oscillation (AO) (Rigor et al., 2002; Deser and Teng, 2008),
the North Atlantic Oscillation (NAO) (Koenigk et al., 2009), and the Pacific Decadal Oscillation (PDO)
35 (Ding et al., 2014), have also been linked to the Arctic sea ice variations and the recent declining trend.
Understanding the relative contributions from these multi-scale natural processes to Arctic sea ice
decline is vital not only for forecasting sea ice conditions but also for projecting climate change and its
impact on the Arctic environment and beyond (Stroeve et al., 2007; Day et al., 2012; Swart et al., 2015;



Ding et al., 2017).

40 In this study, we examine the contributions of changes in large-scale atmosphere and ocean circulations to the trends in Arctic sea ice by applying the Self Organizing Maps (SOM) method (Kohonen, 2001). A relatively new neural network-based method, SOM is superior to some other feature-extracting or clustering methods in that it describes the continuum of atmospheric and oceanic states with a manageable number of representative patterns, as compared to only providing useful information on

45 aggregate patterns by Empirical Orthogonal Function (EOF) and other similar methods. Over the past decade, SOM has been widely used in atmosphere and ocean sciences (Hewitson and Crane, 2002; Leloup et al., 2007; Johnson et al., 2008; Lee et al., 2011; Chu et al., 2012). For example, SOM was used to explain the eastward shift of the North Atlantic Oscillation (NAO) since the late 1970s (Johnson et al., 2008). The SOM approach was also used to examine the contributions of different ENSO flavours to the

50 SST trend in the tropical Pacific Ocean (Johnson, 2013).

We apply SOM to a monthly sea ice concentration dataset for the period 1979 - 2016. We will show how much of the recent declining trend in the Arctic sea ice concentrations may be associated with the low frequency atmospheric circulation modes related to SST anomalies over the Pacific and Atlantic Oceans. Although the analyses have been carried out for all four seasons, we will show the results for autumn

55 only since Arctic sea ice reduction in autumn has strongest influence on the wintertime atmospheric circulations over Eurasia and North America (Francis et al., 2009; Petoukhov and Semenov, 2010; Peings and Magnusdottir, 2014).

2 Dataset and Methods

For the sea ice analysis, we utilized National Snow and Ice Data Center (NSIDC) monthly sea ice

60 concentration dataset that has a horizontal grid of 25 km × 25 km on a polar stereographic projection for the period October 1978 - present (<http://nsidc.org/data/NSIDC-0051>). For the atmospheric circulation analysis, we extracted atmospheric variables from the ERA-Interim reanalysis (Dee et al., 2011) that covers the period 1979-2016 with a horizontal grid spacing of 1.5° latitude by 1.5° longitude, and obtained SST data from the Hadley Center Sea Ice and Sea Surface Temperature dataset (HadISST)

65 (Rayner et al., 2003) (<http://www.metoffice.gov.uk/hadobs/hadisst/>) that is on a 1° latitude by 1° longitude grid for the period 1870 - 2016.

The SOM technique is utilized to extract patterns of Arctic sea ice concentrations. As a neural



network-based method, SOM uses unsupervised learning to determine generalized patterns in complex data. The technique can reduce multidimensional data into two-dimensional array consisting of a matrix
70 of nodes. Each node in the array has a reference vector that displays a spatial pattern of the input data. All patterns in the two-dimensional array represent the full continuum of states in the input data. The SOM algorithm also is a clustering technique, but unlike other clustering techniques, it does not need a priori decisions on data distribution. Unlike the EOF analysis, the SOM technique does not require the orthogonality of two spatial patterns. A detailed description of the SOM algorithm is given in Kohonen
75 (2001).

In this study, the SOM technique was used to categorize anomalous seasonal sea ice concentration patterns north of 50°N for autumn (September-October-November). The autumn seasonal anomalies are calculated by subtracting the climatology, which is the overall mean for all 38 autumns in the study period 1979-2016, from the autumn mean for each year. The anomalous sea ice pattern for each autumn
80 is assigned to the best-matching SOM pattern on the basis of minimum Euclidean distance. Pattern correlations between anomalous sea ice field for each autumn and its corresponding best-matching SOM pattern are used to determine the number of SOM nodes or grids (Lee and Feldstein, 2013). We calculate spatial correlation coefficients for different number of SOM grids ranging from 2×2 to 4×5 (Table 1). There is a large increase in correlation from 2×4 to 3×3 and thus the 3×3 SOM grid is chosen for the
85 analysis. Smaller grids may not adequately capture the variability of autumn Arctic sea ice, whereas larger grids, although providing more details, do not alter the results and conclusions. The contribution of each SOM pattern to trends in Arctic sea ice concentration is calculated by the product of each SOM pattern and its frequency trend (Johnson, 2013), where frequency is calculated by the number of the occurrences of each SOM pattern divided by the total number of autumns over the study period (38) and
90 the trend of the frequency time series for each SOM pattern is determined through linear regression. The sum of the contributions from all SOM patterns represents the trends in Arctic sea ice explained by the SOM patterns, which in this case indicates trends resulting from low-frequency variability. The significance of the trends in the time series for each SOM pattern is tested using the Student's t-test. Residual trends are calculated by subtracting SOM-explained trends from the total trends.

95 **3 SOM results**

Sea ice concentration anomalies occur mainly in the marginal seas from the Barents Sea to the Beaufort Sea, with maximum anomalies in the Barents Sea and the Kara Sea, and over the Beaufort Sea and the East Siberian Sea. Nodes 1, 2 and 4 depict all negative anomalies, whereas Nodes 5, 6, 8 and 9 exhibit all positive anomalies. Nodes 3 and 7, on the other hand, show a mixed pattern with opposite changes in the Barents Sea in the Atlantic sector of the Arctic Ocean and the Beaufort Sea and East Siberian Sea over the Pacific sector. The largest change with similar strength over the Pacific and the Atlantic sectors are depicted by Nodes 1 and 9, and both nodes also have the highest (24%) frequency of occurrences. The other nodes that are either all positive or all negative exhibit larger spatial variability in the strengths of the signals with much stronger signal in either the Atlantic sector (Nodes 2, 5 and 8) or the Pacific sector (Nodes 4 and 6). The two mixed patterns show similar strength over the two sectors, but the pattern with positive anomalies over the Beaufort Sea and the East Siberian Sea and negative anomalies over the Barents Sea, as depicted by Node 3, occurs much more frequently (13%) than the opposite pattern represented by Node 7 (8%).

We examine trends in the frequency of occurrence for each SOM pattern and their contribution to trends in the Arctic autumn sea ice concentration. Figure 2 shows the occurrence time series for each SOM pattern. The nodes with spatially uniform changes appear to be separated into two clusters with those showing all positive anomalies (Nodes 5, 6, 8 and 9) appearing in the 80s and 90s and those having all negative anomalies (Nodes 1 and 4) appearing after 2000. The transition from all positive anomalies in the earlier part, to all negative anomalies in the later part, of the time series is consistent with the trends in the observed Arctic sea ice concentration during the same time period. Not surprisingly, the transition appears to be dominated by the two strongest and most frequent patterns denoted by Node 9 (all positive and occurring from the 1980s through mid 1990s) and Node 1 (all negative and occurring exclusively after 2005). Only these two nodes have linear trends that are statistically significant at above 95% confidence level. The slopes of the trend lines for these two nodes are opposite but the values are similar (0.027 yr⁻¹ for Node 1 and -0.021 yr⁻¹ for Node 9). The other nodes have statistically insignificant trends with magnitudes less than 0.01 yr⁻¹.

The spatial patterns of the trends in anomalous autumn sea ice concentration explained by each node and by all nodes are shown in Figs. 3 and 4. Together, the nine SOM nodes explain about 60% of total trends



in the autumn sea ice loss (Fig. 4b). Among them Node 1 explains the largest portion (33%) of the total
125 trend, followed by Node 9 (21%), with the other 7 nodes together accounting for only 6% of the loss.

4 Potential Mechanisms

To explain the spatial patterns depicted by the two dominant nodes, we made composite maps over the
years of occurrences for Nodes 1 and 9, respectively, and Figs. 5-7 show composite patterns of the
anomalous SST and anomalous atmospheric circulations represented by the 500-hPa geopotential height,
130 850-hPa wind, surface to 750-hPa specific humidity, surface downward longwave radiation, and surface
air temperature. For Node 1, the SST composite pattern resembles negative phase of the PDO in the
North Pacific and positive phase of the AMO in the North Atlantic (Fig. 5). The positive SST anomalies
over the mid-latitude North Pacific produce local negative upper-tropospheric vorticity anomalies
(Hoskins and Karoly, 1981) which excite a wave train with zonal wave number two that propagates
135 eastward to North America, North Atlantic, and Eurasian Continent (Fig. 5). Over the Arctic, the pattern
resembles negative phase AD, with a center of negative 500-hPa height anomalies over Greenland and
the Baffin Bay, and a center of positive anomalies over the Kara Sea. The zonal pressure gradient
between the two centers induces anomalous low-troposphere southwesterly and southerly winds over the
North Atlantic Ocean (Fig. 6) that transport warm and moist air from North Atlantic into the Arctic
140 Ocean north of Eurasia, thus increasing surface air temperature and humidity and reducing sea ice
concentration in the Arctic (Fig. 7). The higher moisture content in the Arctic surface air also facilitates
the occurrence of water vapour and cloud radiative feedback process (Sedlar et al., 2011) during which
increased downward longwave radiation (Fig. 7) enhances surface warming and sea ice melting. The
anomalous high pressure produces subsidence and the adiabatic warming associated with the sinking air
145 contributes to the sea ice loss (Ding et al., 2017) (Not shown). The opposite may occur in the region
under the anomalous low pressure center. But the warm southwesterly winds over the northeastern
Canada also favor the sea ice loss there.

For Node 9, the SST composite is characterized by negative anomalies in both the Pacific and the
Atlantic except for areas of the tropical Pacific and the west coast of North America (Fig.5). The two
150 negative SST anomaly centers over the mid-latitude North Pacific induce positive local
upper-troposphere vorticity anomalies (Hoskins and Karoly, 1981), which generate a wave train of zonal
wave numbers two. There is positive phase AO in the Arctic (Fig.5). Anomalous northeasterly winds in



the North Atlantic Ocean induced by anomalous Icelandic low are unfavourable for warm air intrusion into the Arctic Ocean (Fig. 6), a result also indicated in a previous study (Kim et al., 2017). Despite the
155 occurrences of anomalous southwesterly winds over the Barents Sea and southeasterly winds over the Sea of Okhotsk, the cold advection from anomalous cold sea water prevents the Arctic sea ice from melting. Meanwhile the cold advection also reduces water vapor content in the lower troposphere and the resulting smaller downward longwave radiation facilitates the occurrence of negative surface air temperature and positive Arctic sea ice anomalies north of Eurasia (Fig. 7). The northerly winds over the
160 Beaufort Sea, northeastern Canada and Greenland Sea also contribute to the decrease in surface air temperature and increase in the sea ice concentration.

The opposite patterns in Nodes 1 and 9 may be explained by the differences in the water vapor-radiation feedback process resulting from anomalous temperature and especially water vapour transport by anomalous atmospheric circulations associated with different patterns of SST anomalies over the North
165 Pacific and Atlantic. The patterns of SST anomalies are nearly symmetric for the two nodes over the North Atlantic, but they are somewhat asymmetric over the North Pacific. For Node 1, there is one center of high SST over the central North Pacific, whereas Node 9 is associated with two centers of low SST: one over the Coast of Japan and another in central North Pacific. These differences in the SST anomaly patterns lead to different wave trains and high-latitude atmospheric circulations.

170 The composites here are made based on the frequency time series of the two dominant SOM patterns, which is different from composites based simply on the original sea ice time series. With SOM, lower sea ice years were denoted by 2007-2013 and 2015-2016 while higher sea ice years are represented by 1980-1982, 1986-1989, 1992, and 1996. With original sea ice time series, higher and lower sea ice periods are usually considered as before and after the late 1990s. The SOM-based composites allow for
175 better depiction of atmospheric circulation patterns that have significant impact on sea ice trends.

5 Conclusions

We investigate the potential mechanisms for the autumn Arctic sea ice decline for the period 1979-2016 using the SOM method. Our results show that a large portion of the autumn Arctic sea ice loss may be
180 associated with the changes in the temperature and water vapour transport and the associated water vapour radiation feedback resulting from anomalous atmospheric circulations linked to SST anomalies



over the North Pacific and North Atlantic. This result provides further evidence that the mid-latitude SST anomalies play a vital role in the accelerated Arctic sea ice decline in recent decades (Ding et al., 2017; Yu et al., 2017). An important finding is that the opposite pattern of the Arctic sea ice anomalies during
185 the early (positive) and later (negative) parts of the 1979-2016 period is not associated with opposite phase of an atmospheric circulation mode; but instead the change may be explained by two different atmospheric circulation patterns (AO and AD) associated with an asymmetry in the anomalous SST distributions over the North Pacific. The teleconnections between the Arctic sea ice variability and mid-latitude SST anomalies suggest that on a decadal or longer time scale it may be necessary to include
190 the Arctic sea ice and mid-latitude SST interactions or feedbacks in any investigations of Arctic warming and sea ice decline and their potential influence on mid-latitude weather and climate, an area of active research in recent years (Barnes and Screen, 2015; Overland and Wang, 2015; Francis and Skific, 2015). Finally, the results here help highlight the large contributions from the decadal-scale natural climate variability to Arctic climate change, though further studies using coupled global atmosphere-ocean-sea
195 ice models are necessary to fully understand the physical mechanisms.

Data Availability

All data used in the current study are publicly available. The monthly sea ice concentration data are available from the National Snow and Ice Data Center (NSIDC) (<http://nsidc.org/data/NSIDC-0051>), the ERA-Interim reanalysis data are available from the European Center for Mid-Range Weather
200 Forecasting (<https://www.ecmwf.int/en/forecasts/datasets/reanalysis-datasets/era-interim>) and the SST data are available from the Hadley Centre for Climate Prediction and Research (<http://www.metoffice.gov.uk/hadobs/hadisst/>).

Competing interests

The authors declare that they have no conflict of interest.

205 Author Contributions

L. Yu designed the study, with input from S. Zhong, and carried out the analyses. L. Yu and S. Zhong prepared the manuscript.



Acknowledgements

This study is supported by The National Key Research and Development Program of China
210 (No.YS2017YFGH000085).

References

- Barnes, E. A., and Screen, J.: The impact of Arctic warming on the midlatitude jet stream: Can it? Has it? Will it? WIREs Clim. Change, 6, 277-286, <https://doi.org/10.1002/wcc.337>, 2015.
- Bintanja, R., Graverson, R. G., and Hazeleger, W.: Arctic winter warming amplified by the thermal
215 inversion and consequent low infrared cooling to space, Nat. Geosci., 4, 758-761,
<https://doi.org/10.1038/ngeo1285>, 2011.
- Chu, J.-E., Hameed, S. N., and Ha, K.-J.: Non-linear intraseasonal phases of the East Asian summer monsoon: Extraction and analysis using self-organizing maps, J. Climate, 25, 6975-6988,
<https://doi.org/10.1175/JCLI-D-11-00512.1>, 2012.
- 220 Day, J. J., Hargreaves, J. C., Annan, J. D., and Abe-Ouchi, A.: Sources of multidecadal variability in Arctic sea ice extent, Environ. Res. Lett., 7, 034011, <https://doi.org/10.1088/1748-9326/7/7/034011>,
2012.
- Dee, D. P., Uppala, S. M., Simmons, A. J., Berrisford, P., Poli, P., Kobayashi, S., Andrae, U.,
Balmaseda, M. A., Balsamo, G., Bauer, P., Bechtold, P., Beljaars, A. C. M., van de Berg, L.,
225 Bidlot, J., Bormaan, N., Delsol, C., Dragani, R., Fuentes, M., Geer, A. J., Haimberger, L., Healy, S. B., Hersbach, H., Hólm, E. V., Isaksen, I., Kållberg, P., Köhler, M., Matricardi, M., McNally, A. P., Mong-Sanz, B. M., Morcrette, J.-J., Park, B.-K., Peubey, C., de Rosnay, P., Tavolato, C., Thépaut, J.-N., and Vitart, F.: The ERA-Interim reanalysis: configuration and performance of the data assimilation system, Q. J. R. Meteorol. Soc., 137, 553-597, <https://doi.org/10.1002/qj.828>,
230 2011.
- Deser, C., and Teng, H.: Evolution of Arctic sea ice concentration trends and the role of atmospheric circulation forcing, Geophys. Res. Lett., 35, L02504, <https://doi.org/10.1029/2007GL032023>,
2008.
- Ding, Q., Wallace, J. M., Battisti, D. S., Steig, E. J., Gallant, A. J. E., Kim, H.-J., and Geng, L.:
235 Tropical forcing of the recent rapid Arctic warming in northeastern Canada and Greenland, Nature, 509, 209-212, <https://doi.org/10.1038/nature13260>, 2014.



- Ding, Q., Schweiger, A., L'Heureux, M., Battisti, D. S., Po-Chedley, S., Johnson, N. C.,
Blanchard-Wrigglesworth, E., Harnos, K., Zhang, Q., Eastman, R., and Steig, E. J.: Influence of
high-latitude atmospheric circulation changes on summertime Arctic sea ice, *Nat. Clim. Change*, 7,
240 289-295, <https://doi.org/10.1038/NCLIMATE3241>, 2017.
- Flanner, M. G., Shell, K. M., Barlage, M., Perovich, D. K., and Tschudi, M. A.: Radiative forcing and
albedo feedback from the Northern Hemisphere cryosphere between 1979 and 2008, *Nat. Geosci.*,
4, 151–155, <https://doi.org/10.1038/NGEO1062>, 2011.
- Francis, J. A., Chan, W., Leathers, D. J., Miller, J. R., and Veron, D. E.: Winter Northern Hemisphere
245 weather patterns remember summer Arctic sea-ice extent, *Geophys. Res. Lett.*, 36, L07503,
<https://doi.org/10.1029/2009GL037274>, 2009.
- Francis, J. A., and Skific, N.: Evidence linking rapid Arctic warming to mid-latitude weather patterns,
Phil. Trans. R. Soc. A., 373, 20140170, <https://doi.org/10.1098/rsta.2014.0170>, 2015.
- Gagné, M., -È., Gillett, N. P., and Fyfe, J. C.: Impact of aerosol emission controls on future arctic se ice
250 cover, *Geophys. Res. Lett.*, 42, 8481-8488, <https://doi.org/10.1002/2015GL065504>, 2015.
- Hewitson, B. C., and Crane, R. G.: Self-organizing maps: Applications to synoptic Climatology, *Clim.*
Res., 22, 13-26, 2002.
- Hoskins, B. J., and Karoly, D. J.: The steady linear response of a spherical atmosphere to thermal and
orographic forcing, *J. Atmos. Sci.*, 38, 1179-1196.
- 255 Johnson, N. C., Feldstein, S. B., and Tremblay, B.: The continuum of Northern Hemisphere
teleconnection patterns and a description of the NAO shift with the use of self-organizing maps, *J.*
Climate, 21, 6354-6371, <https://doi.org/10.1175/2008JCLI2380.1>, 2008.
- Johnson, N. C.: How many ENSO flavors can we distinguish?, *J. Climate*, 26, 4816-4827,
<https://doi.org/10.1175/JCLI-D-12-00649.1>, 2013.
- 260 Kim, B.-M., Hong, J.-Y., Jun, S.-Y., Zhang, X., Kwon, H., Kim, S.-J., Kim, J.-H., Kim, S.-W., and
Kim, H.-K.: Major cause of unprecedented arctic warming in January 2016: Critical role of an
Atlantic windstorm, *Sci. Rep.*, 7, 40051, <https://doi.org/10.1038/srep40051>, 2017.
- Koenigk, T., Mikolajewicz, U., Jungclaus, J., and Kroll, A.: Sea ice in the Barents Sea: Seasonal to
interannual variability and climate feedbacks in a global coupled model, *Clim. Dyn.*, 32,
265 1119–1138, <https://doi.org/10.1007/s00382-008-0450-2>, 2009.
- Kohonen, T. (Eds): Self-organizing maps, 3rd ed. Springer, Berlin, Germany, 501pp., 2001.



- Kug, J.-S., Jeong, J.-H., Jang, Y.-S., Kim, B.-M., Folland, C. K., Min, S.-K., and Son, S.-W.: Two distinct influences of Arctic warming on cold winters over North America and East Asia, *Nat. Geosci.*, 8, 759-762, <https://doi.org/10.1038/NGEO2517>, 2015.
- 270 Lee, S., and Feldstein, S. B.: Detecting ozone-and greenhouse gas-driven wind trends with observational data, *Science*, 339, 563-567, <https://doi.org/10.1126/science.1225154>, 2013.
- Lee, S. T., Gong, T., Johnson, N. C., Feldstein, S. B., and Pollard, D.: On the possible link between tropical convection and the Northern Hemisphere Arctic surface air temperature change between 1958 and 2001, *J. Climate*, 24, 4350-4367, <https://doi.org/10.1175/2011JCLI4003.1>, 2011.
- 275 Leloup, J., Lachkar, Z., Boulanger, J.-P., and Thiria, S.: Detecting decadal changes in ENSO using neural networks, *Clim. Dyn.*, 28, 147-162, <https://doi.org/10.1007/s00382-006-0173-1>, 2007.
- Min, S.-K., Zhang, X., Zwiers, F. W., and Agnew, T.: Human influence on arctic sea ice detectable from early 1990s onwards, *Geophys. Res. Lett.*, 35, 213-36, <https://doi.org/10.1029/2008GL035725>, 2008.
- Mori, M., Watanabe, M., Shiogama, H., Inoue, J., and Kimoto, M.: Robust Arctic sea-ice influence on the frequent Eurasian cold winters in past decades, *Nat. Geosci.*, 7, 869-873, <https://doi.org/10.1038/NGEO2277>, 2014.
- 280 Notz, D., and Marotzke, J.: Observations reveal external driver for Arctic sea-ice retreat, *Geophys. Res. Lett.*, 39, 89-106, <https://doi.org/10.1029/2012GL051094>, 2012.
- Overland, J. E., and Wang, M.: Increased variability in the early winter subarctic North American atmospheric circulation, *J. Climate*, 28, 7297-7305, <https://doi.org/10.1175/JCLI-D-15-0395.1>, 2015.
- 285 Park, W., and Latif, M.: Multidecadal and multicentennial variability of the meridional overturning circulation, *Geophys. Res. Lett.*, 35, L22703, <https://doi.org/10.1029/2008GL035779>, 2008.
- Parkinson, C. L.: Global sea ice coverage from satellite data: Annual cycle and 35-Yr trends, *J. Climate*, 27, 9377-9382, <https://doi.org/10.1175/JCLI-D-14-00605.1>, 2014.
- 290 Peings, Y., and Magnusdottir, G.: Response of the wintertime Northern Hemisphere atmospheric circulation to current and projected Arctic sea ice decline: a numerical study with CAM5, *J. Climate*, 27, 244-264, <https://doi.org/10.1175/JCLI-D-13-00272.1>, 2014.
- Petoukhov, V., and Semenov, V. A.: A link between reduced Barents-Kara sea ice and cold winter extremes over northern continents, *J. Geophys. Res.*, 115, D21111, <https://doi.org/10.1029/JD013568>, 2010.
- 295



- Pithan, F., and Mauritsen, T.: Arctic amplification dominated by temperature feedbacks in contemporary climate models, *Nat. Geosci.*, 7, 181-184, <https://doi.org/10.1038/NGEO2071>, 2014.
- Post, E., Bhatt, U. S., Bitz, C. M., Brodie, J. F., Fulton, T. L., Hebblewhite, M., Kerby, J., Kutz, S. J.,
300 Stirling, I., and Walker, D. A.: Ecological consequences of sea-ice decline, *Science*, 341,
519–524, <https://doi.org/10.1126/science.1235225>, 2013.
- Rayner, N. A., Parker, D. E., Horton, E. B., Folland, C. K., Alexander, L. V., Rowell, D. P., Kent, E.
C., and Kaplan, A.: Global analyses of sea surface temperature, sea ice, and night marine air
temperature since the late nineteenth century, *J. Geophys. Res.*, 108, 4407,
305 <https://doi.org/10.1029/2002JD002670>, 2003.
- Rigor, I., Wallace, J. M., and Colony, R. L.: Response of sea ice to the Arctic Oscillation, *J. Climate*, 15,
2648–2663, [https://doi.org/10.1175/1520-0442\(2002\)015<2648:ROSITT>2.0.CO;2](https://doi.org/10.1175/1520-0442(2002)015<2648:ROSITT>2.0.CO;2), 2002.
- Rothrock, D. A., Yu, Y., and Maykut, G. A.: Thinning of the Arctic sea-ice cover, *Geophys. Res. Lett.*,
26, 3469–3472, 1999.
- 310 Sedlar, J., Tjernström, M., Mauritsen, T., Shupe, M. D., Brooks, I. M., Persson, P. Ola G., Birch, C. E.,
Leck, C., Sirevaag, A., and Nicolaus, M.: A transitioning Arctic surface energy budget: the
impacts of solar zenith angle, surface albedo and cloud radiative forcing, *Clim. Dyn.*, 37,
1643-1660, <https://doi.org/10.1007/s00382-010-0937-5>, 2011.
- Stroeve, J., Holland, M., Meier, W., Scambos, T., and Serreze, M.: Arctic sea ice decline: Fast than
315 forecast, *Geophys. Res. Lett.*, 34, L09501, <https://doi.org/10.1029/2007GL029703>, 2007.
- Swart, N. C., Fyfe, J. C., Hawkins, E., Kay, J. E., and Jahn, A.: Influence of internal variability on Arctic
sea-ice trends, *Nat. Clim. Change*, 5, 86-89, 2015.
- Wang, J., Zhang, J., Watanabe, E., Ikeda, M., Mizobata, K., Walsh, J. E., Bai, X., and Wu, B.: Is the
Dipole anomaly a major driver to record lows in Arctic summer sea ice extent?, *Geophys. Res.*
320 *Lett.*, 36, L05706, <https://doi.org/10.1029/2008GL036706>, 2009.
- Yu, L., Zhong, S., Winkler, J. A., Zhou, M., Lenschow, D. H., Li, B., Wang, X., and Yang, Q.: Possible
connections of the opposite trends in Arctic and Antarctic sea-ice cover, *Sci. Rep.*, 7, 45804,
<https://doi.org/10.1038/srep45804>, 2017.

325



Table 1. The 38-year (1979-2016) average of spatial correlations between the seasonal Arctic sea ice concentration and the corresponding SOM pattern for each year.

| SOM grids | 2×2 | 2×3 | 2×4 | 3×3 | 3×4 | 3×5 | 4×4 | 4×5 |
|--------------------------|------|------|------|------|------|------|------|------|
| Correlation coefficients | 0.59 | 0.56 | 0.59 | 0.64 | 0.66 | 0.69 | 0.68 | 0.70 |



Figure captions

Fig. 1. The SOM patterns of anomalous autumn (September–November) Arctic sea ice concentration for a 3×3 grid for the 1979–2016 period. The percentages at the top left of each panel indicate the frequency of occurrence of the pattern.

Fig. 2. Occurrence time series for each SOM pattern in Fig. 1.

Fig. 3. Trends in the anomalous autumn Arctic sea ice concentration explained by each SOM pattern (Units: yr⁻¹).

Fig. 4. Total (a), SOM-explained (b) and residual (c) trends (Units: yr⁻¹) in the anomalous autumn Arctic sea ice concentration fields. Dots in (a) indicate above 90% confidence level.

Fig. 5. Composites of anomalous sea surface temperature (°C) and 500-hPa geopotential height (gpm) for nodes 1 and 9. Dotted regions denote above 90% confidence level.

Fig. 6. The same as Fig. 5, but for anomalous 850-hPa wind field. Shaded regions denote above 90% confidence level.

Fig. 7. The same as Fig. 5, but for anomalous integrated atmospheric water vapor from surface to 750 hPa (g kg⁻¹), accumulated surface downward longwave radiation (W m⁻² × 10⁵) and surface air temperature (°C). Dotted regions denote above 90% confidence level.

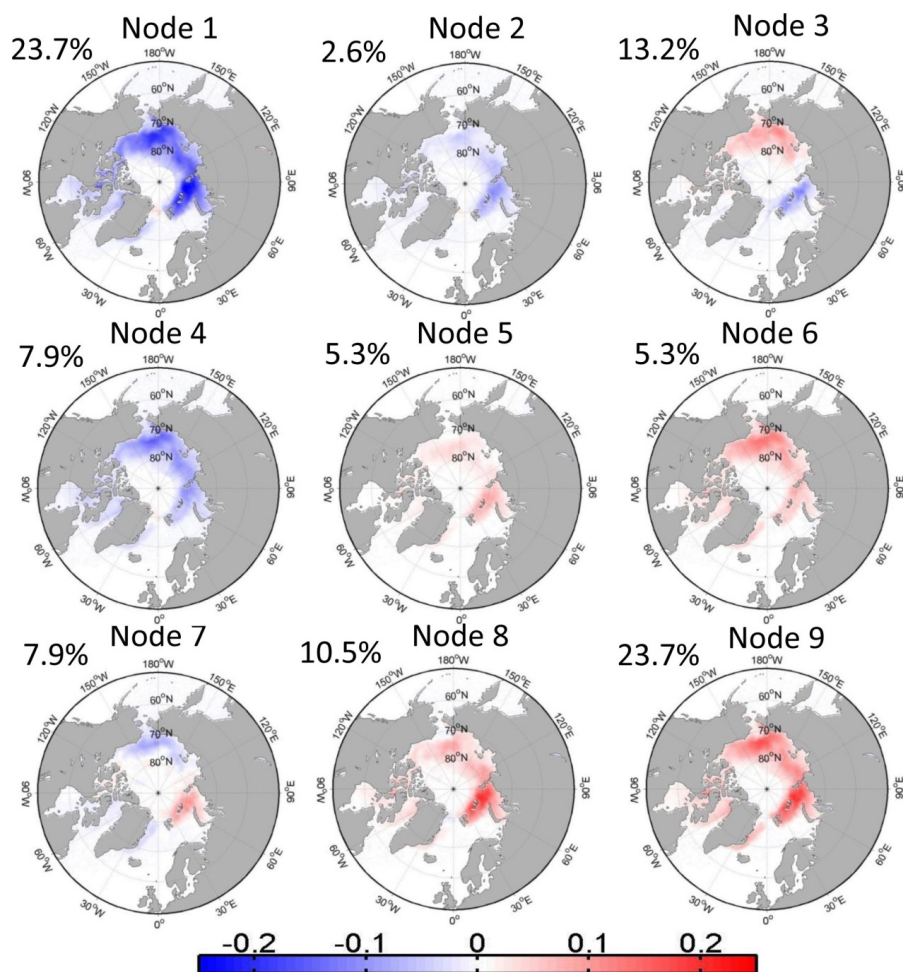


Figure 1 The SOM patterns of the anomalous autumn (September–November) Arctic sea ice concentration for a 3×3 grid for the 1979–2016 period. The percentages at the top left of each panel indicate the frequency of occurrence of the pattern.

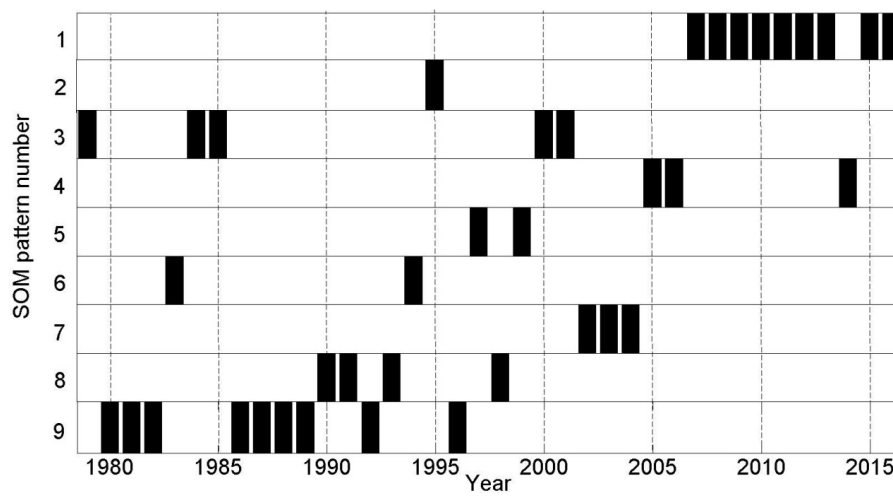


Figure 2. Occurrence time series for each SOM pattern in Figure 1.

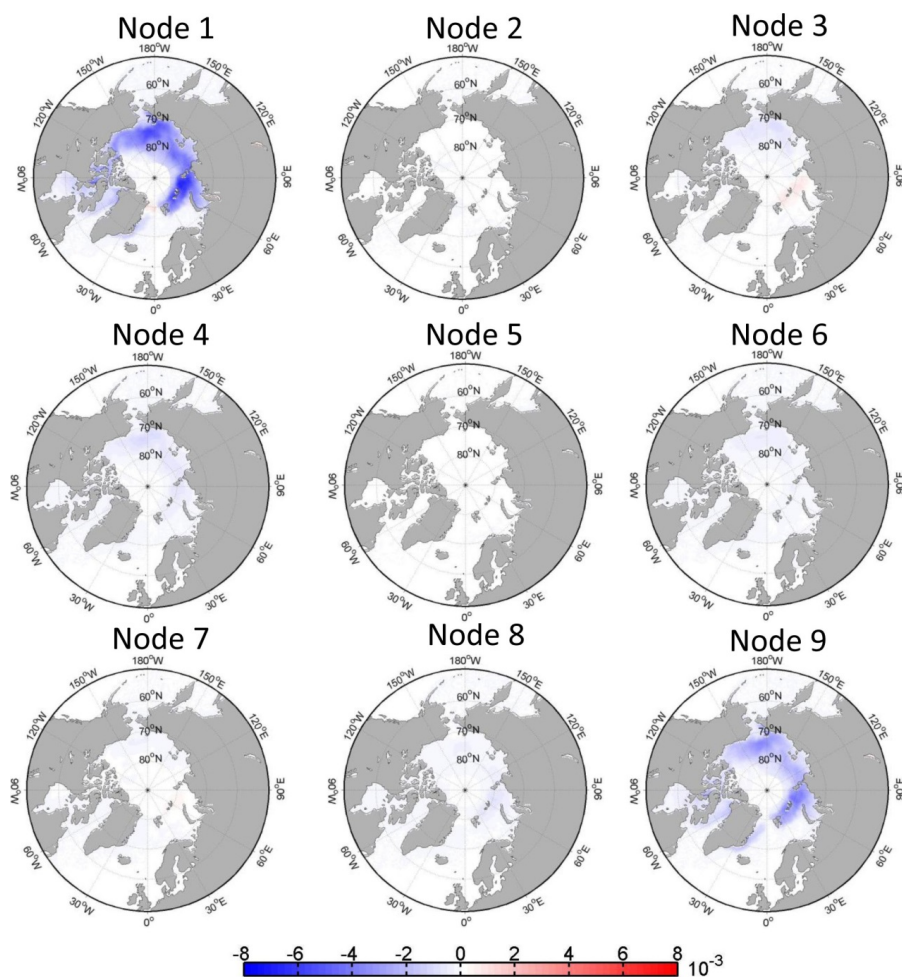


Figure 3. Trends in the anomalous autumn Arctic sea ice concentration explained by each SOM pattern (Units: yr^{-1}).

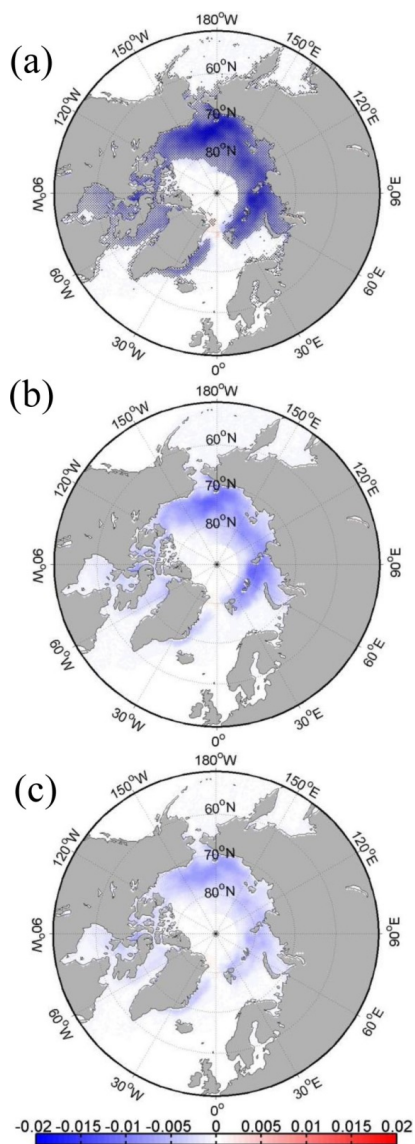


Figure 4. Total (a), SOM-explained (b) and residual (c) trends (Units: yr^{-1}) in the anomalous autumn Arctic sea ice concentration fields. Dots in (a) indicate above 95% confidence level.

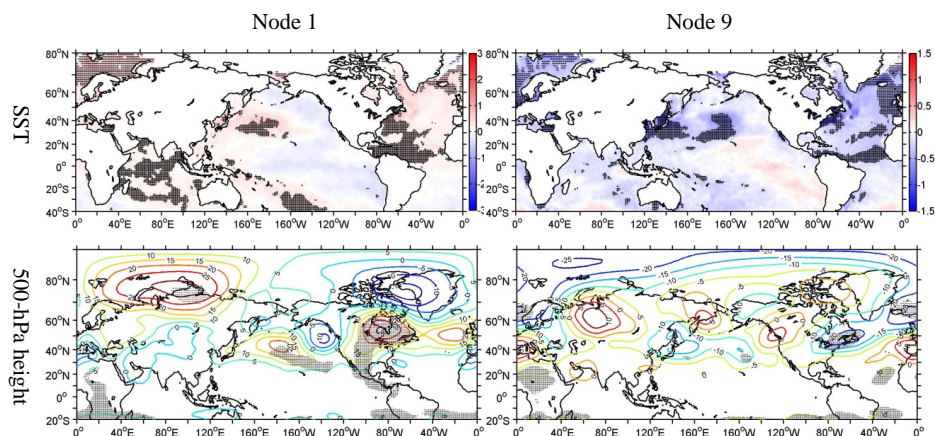


Figure 5. Composites of anomalous sea surface temperature ($^{\circ}\text{C}$) and 500-hPa geopotential height (gpm) for nodes 1 and 9. Dotted regions denote above 90% confidence level.

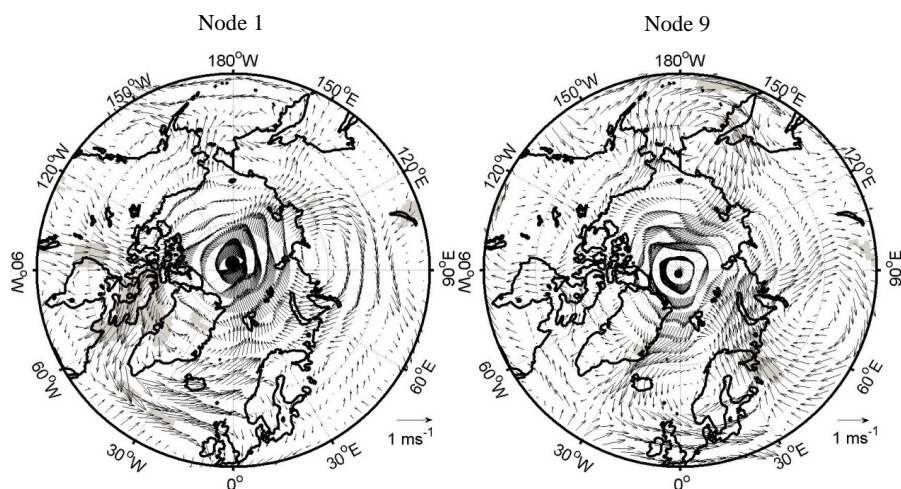


Figure 6. The same as Figure 5, but for anomalous 850 hPa wind field. Shaded regions denote above 90% confidence level.

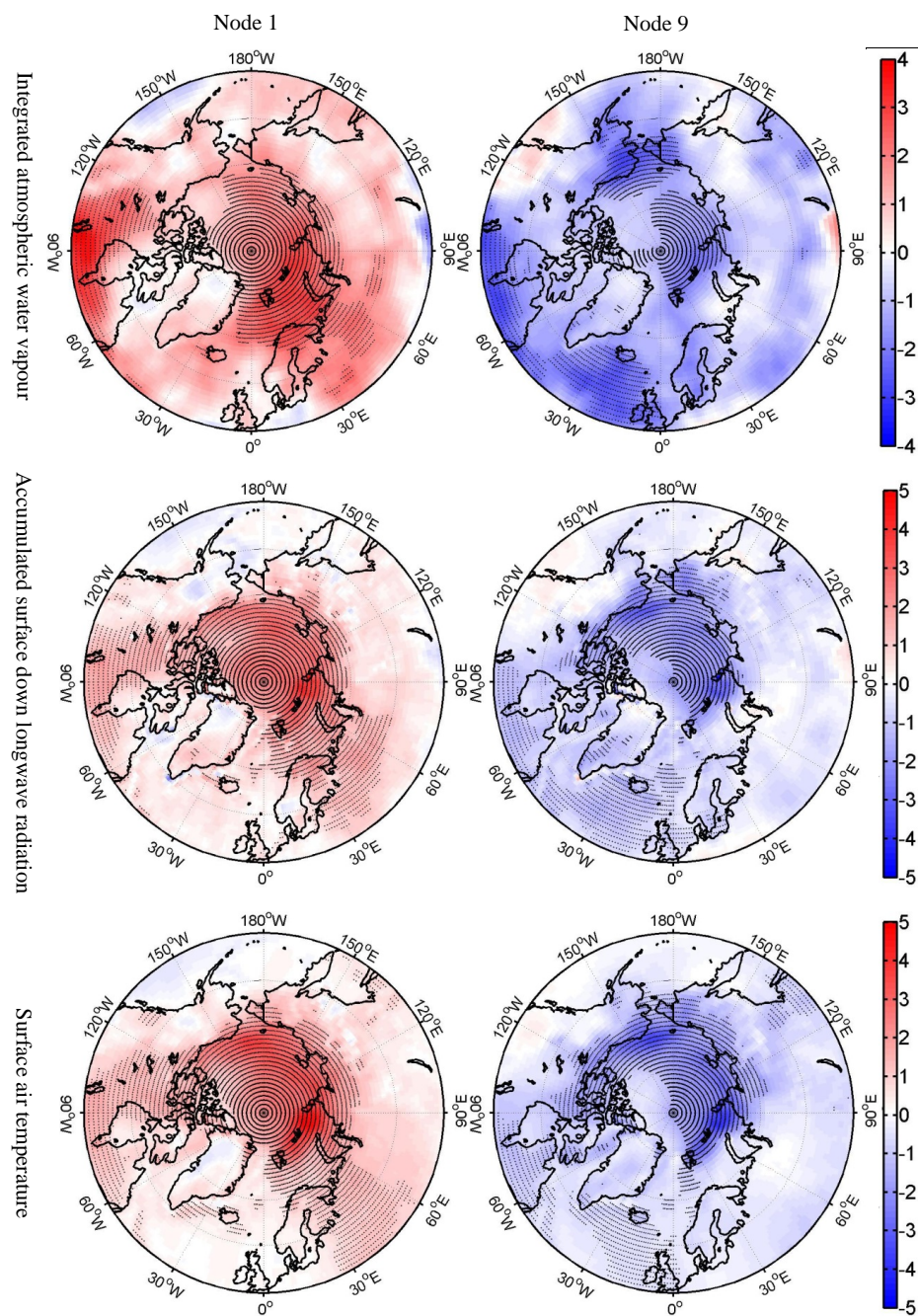


Figure 7. The same as Figure 5, but for anomalous integrated atmospheric water vapor from surface to 750 hPa (g kg^{-1}), accumulated surface downward longwave radiation (10^5Wm^{-2}), and surface air temperature ($^{\circ}\text{C}$). Dotted regions denote above 90% confidence level.